ISSN 1349-1121
JAXA-RM-13-008E

JAXA Research and Development Memorandum

Rotordynamic Fluid Forces of Floating Ring Seal for Rocket Turbopump

Jun HIROMATSU, Masaharu UCHIUMI, Satoshi TAKADA, Naoki NAGAO,
Masato EGUCHI and Hideyuki INOUE

October 2013

Japan Aerospace Exploration Agency

Rotordynamic Fluid Forces of Floating Ring Seal for Rocket Turbopump*

Jun HIROMATSU[*1], Masaharu UCHIUMI[*1], Satoshi TAKADA[*1], Naoki NAGAO[*1], Masato EGUCHI[*2] and Hideyuki INOUE[*3]

ABSTRACT

A floating ring seal (FRS) has been employed as a noncontact type seal, which seals in high-pressure liquid oxygen for the rocket engine turbopump. The turbopump, high-speed, high-power turbomachinery, has suffered from rotor vibration problems up to the present time. However, as the dynamic behavior of FRS has rarely been focused on, it is necessary to clarify the rotordynamic (RD) fluid forces of FRS. The objectives of the present study were to evaluate the RD fluid forces of FRS analytically (bulk-flow model) and experimentally, and to elucidate the structural behavior of FRS caused by the whirling motion of the rotor. Evaluation of RD fluid forces was attempted, and development of a program for evaluation of the FRS is now in progress. RD fluid forces of FRS were measured by an experimental apparatus with an active magnetic bearing. These forces had no significant impact on rotordynamic stability. The axial force induced by differential pressure presses the floating-ring (FR, the component of the FRS) against the stationary housing. Because of the increasing friction force of the secondary contact surface, high axial loads increase the radial force required to reposition the FR. Therefore, it is very important to investigate rotordynamic forces as tribological behavior.

Keywords:
Floating ring seal, Whirling motion, Rotordynamic forces, Bulk-flow model, Stribeck curve

INTRODUCTION

A shaft seal system for a liquid oxygen (LOX) turbopump is one of the most critical components on a liquid rocket engine, and has been employed in the LOX turbopump of the LE-7A engine for the Japanese H-2A and H-2B rockets. A cut model of the LOX turbopump for the LE-7 engine is shown in Fig. 1.

The rocket turbopump is high-speed, high-power turbomachinery, which has suffered from various rotor vibration problems due to high-speed, high-power and high-energy density. Ball

* Received 5 July 2013

*1 Engine System R&D Group, Space Transportation Propulsion R&D Center, Space Transportation Mission Directorate

*2 EBARA CORPORATION

*3 EAGLE INDUSTRY CO., LTD.

bearing stiffness is generally acknowledged to affect rotor vibration characteristics. Thus, the rotor system of the rocket turbopump must be designed in consideration of the effects of the small clearance between the spinning components and the stationary elements to prevent unstable vibration. RD fluid forces which increase due to the small clearances of each component have a significant impact on rotordynamic stability. Especially, the tangential fluid force may act as a destabilizing effect on the rotor. Thus, the objectives of the present study were to evaluate the rotordynamic coefficients of FRS analytically (bulk-flow model) and experimentally, and to elucidate the structural behavior of the FRS caused by the whirling rotor. The FRS is employed as a noncontact type seal between the spinning rotor and stator of the LOX turbopump, and the FR maintains a controlled seal clearance to the rotor under all operating conditions. The studies of FRS for the LOX turbopump have been conducted [1]. Plain annular seals are known to have a significant impact on rotordynamic stability, and RD fluid forces of these plain annular seals have often been reported [2]. However, the dynamic behavior of the FRS has rarely been focused on, and thus it is necessary to clarify RD fluid forces of the FRS. Accurate data are needed to predict and prevent unstable vibration, and it is even more essential to design a stable rotor system using multidisciplinary optimal design based on dynamics design for a rocket engine turbopump [3].

This paper describes the analytic results obtained by the bulk-flow model and the experimental results to clarify RD fluid forces and the structural behavior of the FRS caused by the whirling rotor. Development of a program for evaluation of the FRS is now in progress, and RD fluid forces of a fixed ring seal (non-floating, the same shape as the FRS) were evaluated. Rotordynamic performance tests with active magnetic bearings were conducted under experimental conditions, and RD fluid forces and the structural behavior of the FRS were evaluated. In addition, the fixed ring seal was made, and RD fluid forces of the fixed ring seal were measured. The analytic RD fluid forces of the fixed ring seal were compared with the test results.

A SHAFT SEAL SYSTEM IN THE LIQUID OXYGEN TURBOPUMP

Since the LE-7 rocket engine uses a staged-combustion cycle with a high chamber pressure (13 MPa), the pump delivery pressure and turbine-drive gas pressure are extremely high. The turbine-drive gas, generated at a preburner, is a combustion gas enriched with hydrogen. Therefore, the use of the LOX turbopump shaft seal system is very important for preventing LOX and the high-pressure turbine-drive hot gas from mixing during high-speed operations (18,000 to 20,000 rpm). The shaft seal system of the LOX turbopump is schematically shown in Fig. 2 [4]. The seal system consists of the following seals: a LOX seal comprising a carbon floating-ring and a Kel-F (polychlorotrifluoroethylene) wear-ring, which seals in high-pressure LOX (approximately 4.5 MPa); a turbine gas seal comprising two carbon floating-rings, which seals in high-pressure and low-temperature hydrogen gas (approximately 15 MPa, 170K); and a helium purge seal comprising two carbon segmented circumferential seal rings, which completely prevents LOX and leaked hydrogen gas from mixing. This paper describes experimental results of a rotordynamic performance tests of a carbon FRS in a LOX seal.

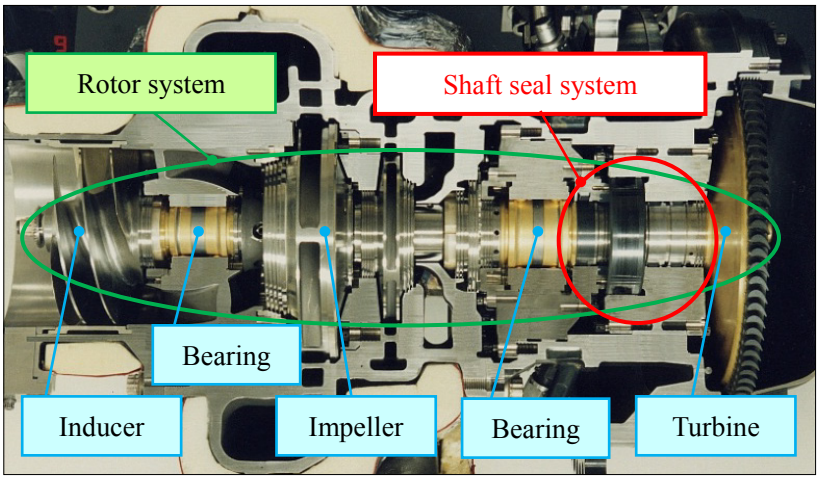

Fig. 1 Layout of major spinning components of the LE-7 LOX turbopump

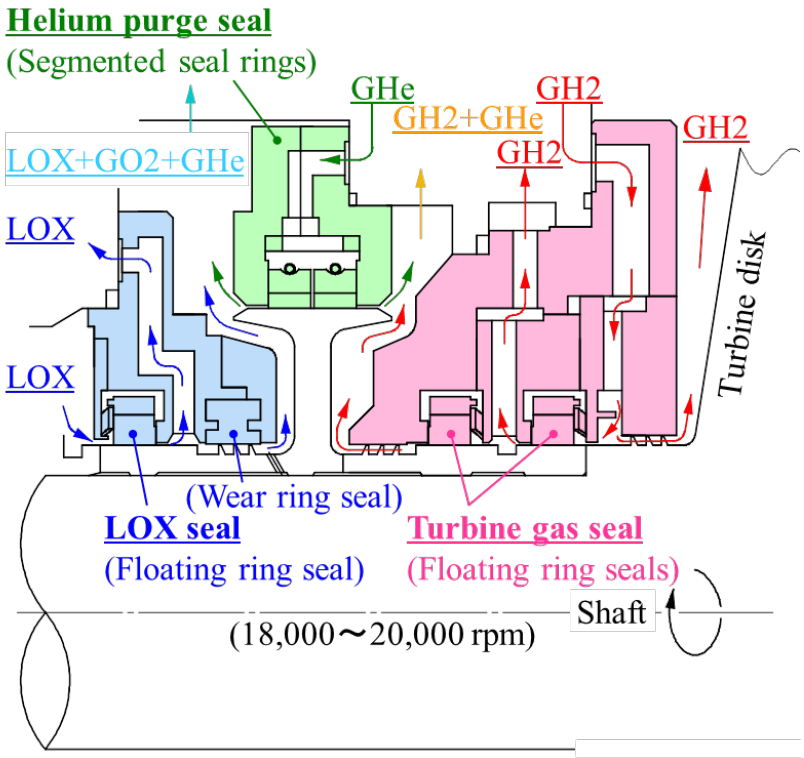

Fig. 2 Shaft seal system of LE-7A LOX turbopump [4]

ROTORDYNAMIC FLUID FORCES

RD fluid reaction force (F) is decomposed into the radial force (Fr) and the tangential force (Ft). Fr is defined as positive outward and Ft as positive in the direction of spinning ω, as shown in Fig. 3. For small whirling motion about a centered position, the relation between RD fluid forces and whirling motion may be expressed by Eq. (1) and Eq. (2) [2, 5].

$$Fr = e\,(\,M\,\Omega^2 - c\,\Omega - K\,) \tag{1}$$

$$Ft = e\,(\,-m\,\Omega^2 - C\,\Omega + k\,) \tag{2}$$

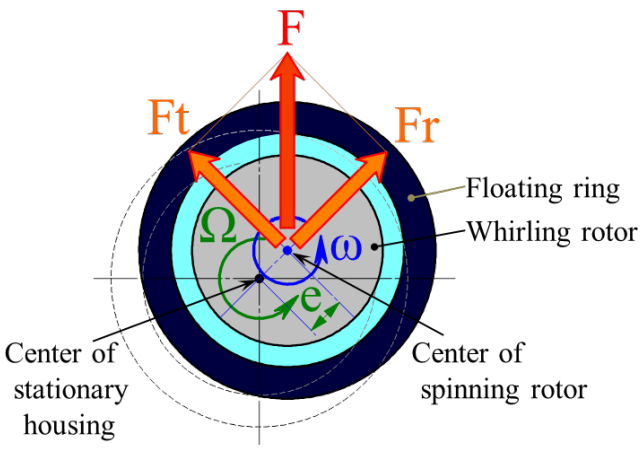

Fig. 3 Definition of RD fluid forces Fr (radial) and Ft (tangential)

The tangential force Ft directly has greater effects on the stability of the rotor. Clearly, the positive tangential force Ft has a destabilizing effect due to the production of a force in the direction of forward whirling motion. The cross-coupled added mass (virtual mass) coefficient m has been dropped as being negligible in comparison with the influence of the destabilizing cross-coupled stiffness coefficient k and the stabilizing direct damping coefficient C. The stability of the rotor depends on k and C, as shown in Fig. 4.

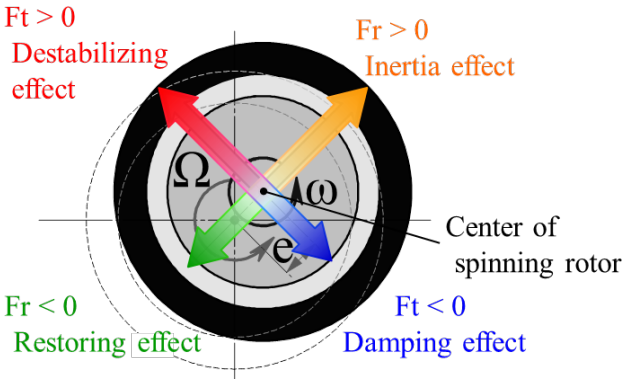

Fig. 4 Effects of RD fluid forces under forward whirling motion ($0 < \Omega/\omega$) of the rotor

BULK-FLOW GOVERNING EQUATIONS MODEL

Evaluation of the radial and tangential forces was attempted, and development of a program for evaluation of the FRS is now in progress including the FR and friction force of secondary sealing surface. RD fluid forces of the fixed ring seal (non-floating) were evaluated, this ring seal having the same shape as the FRS. The governing equations were formulated with the bulk-flow model and a friction factor, as shown in Fig. 5 [5, 6] and Eq. (3) - (5).

Incompressible-flow continuity equation

$$\frac{\partial h}{\partial t}+\frac{1}{R}\frac{\partial (hu)}{\partial \theta}+\frac{\partial (hw)}{\partial z}=0 \qquad (3)$$

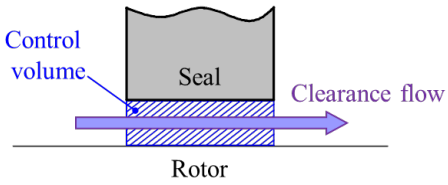

Fig . 5 Flow model in the fixed ring seal

Axial-momentum equation

$$\rho h\left(\frac{\partial w}{\partial t}+\frac{u}{R}\frac{\partial w}{\partial \theta}+w\frac{\partial w}{\partial z}\right)=-h\frac{\partial p}{\partial z}-\frac{\rho}{2}w(f_s V_s+f_r V_r) \qquad (4)$$

Circumferential-momentum equation

$$\rho h\left(\frac{\partial u}{\partial t}+\frac{u}{R}\frac{\partial u}{\partial \theta}+w\frac{\partial u}{\partial z}\right)=-\frac{h}{R}\frac{\partial p}{\partial \theta}-\frac{\rho}{2}\{f_s u V_s+f_r(u-R\omega)V_r\} \qquad (5)$$

The bulk-flow velocities relative to the seal and rotor walls are indicated by the spinning speed, the mean circumferential and axial velocity, as shown in Eq. (6) - (7).

$$V_s=(w^2+u^2)^{\frac{1}{2}} \qquad (6)$$

$$V_r=\{w^2+(u-R\omega)^2\}^{\frac{1}{2}} \qquad (7)$$

Friction factor definitions

Hirs's equations yield the following seal and rotor friction factor, as shown Eq. (8) - (9) [7]. Empirical coefficients (n_s, m_s, n_r, m_r) characterize the flow resistance characteristics of the seal and rotor surface roughness. The present study used the following smooth surface coefficients [5].

$$f_s=n_s\left(\frac{2\rho h V_s}{\mu}\right)^{m_s} \qquad (8)$$

$$f_r=n_r\left(\frac{2\rho h V_r}{\mu}\right)^{m_r} \qquad (9)$$

$m_s = m_r = -0.25,\ n_s = n_r = 0.079$

ANALYTICAL RESULTS

RD fluid forces of the fixed ring seal, which is a non-floating ring and has the same shape as the FRS, were calculated with bulk-flow theory, as shown in Fig. 6.

All of the radial forces were clearly in the region of the restoring effect. The Lomakin effect should have reacted with the rotor because the initial controlled seal clearance to the rotor was very small. Since the cross-coupled added mass coefficient m is almost always negligible, the stability of the rotor depends on the destabilizing cross-coupled stiffness coefficient k and the stabilizing direct damping coefficient C. The tangential forces Ft were not the curved lines from the origin of the coordinate axes, the destabilizing effects of all whirl eccentricities were within approximately $0 < \Omega/\omega < 0.3$. The Y–intercepts of all tangential forces indicated the positive cross-coupled stiffness coefficients k, that is, the destabilizing forces must react with the rotor. The cross-coupled stiffness coefficients k increased with the increase of whirl eccentricities e. However, the restoring effect of the radial fluid forces and the damping effect of the tangential forces increased with the increase of whirl eccentricities e.

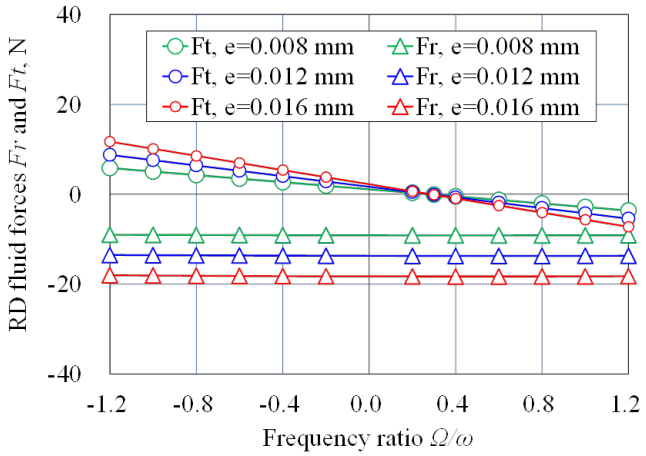

Fig. 6 Calculated RD fluid forces in radial direction (Fr) and tangential direction (Ft) of fixed ring seal (non-floating ring) with bulk-flow theory (dP=1.0 MPa, ω=2,700 rpm, Preswirl velocity=0 m/s)

EXPERIMENTAL APPARATUS

Rotordynamic test stand

Rotordynamic performance tests were conducted with an Ebara rotordynamic test stand (EBARTS) [8], as shown in Fig. 7. This test stand is built vertically on the floor. Feedback control by magnetic bearings for five degrees of freedom with the exception of the spinning direction enables measurement under non-contact state conditions by levitating a rotor from the stationary structure. Consequently, very small RD fluid forces of seals can be measured with precision due to the absence of other elements that may influence measurement. Working fluid (water) was provided from the inlet port of the high-pressure side, and leaked fluid was drained from the outlet port of the low-pressure side. A reinforced plate with windows on the transparent top acrylic plate is needed for observation of the structural behavior of the FRS caused by the whirling rotor, as shown in Fig. 8. The preassembly rotor and FRS are shown in Fig. 9.

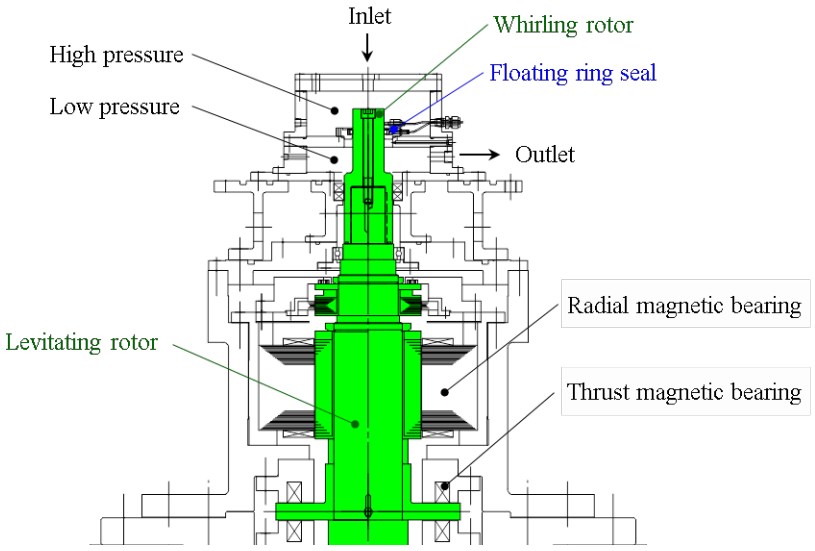

Fig. 7 FRS test configuration of EBARTS with an active magnetic bearing

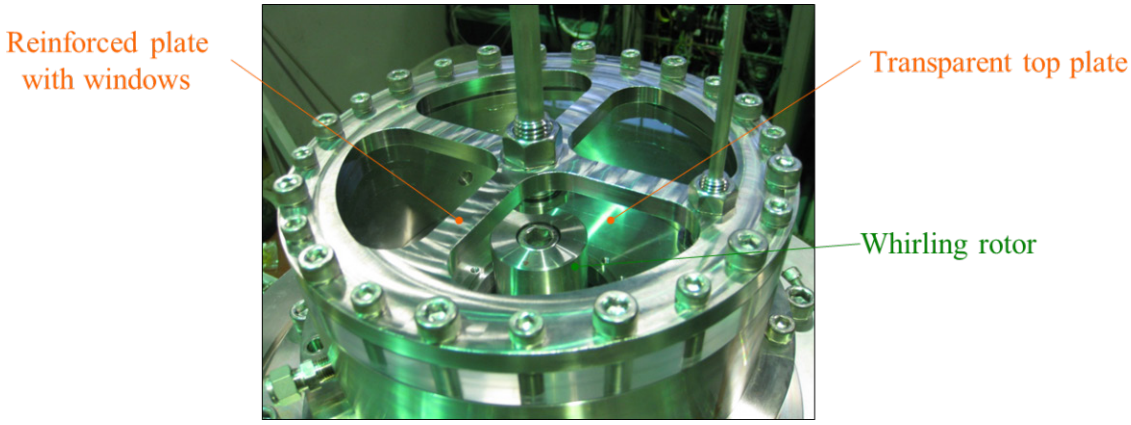

Fig. 8 Transparent top plate and reinforced plate with windows

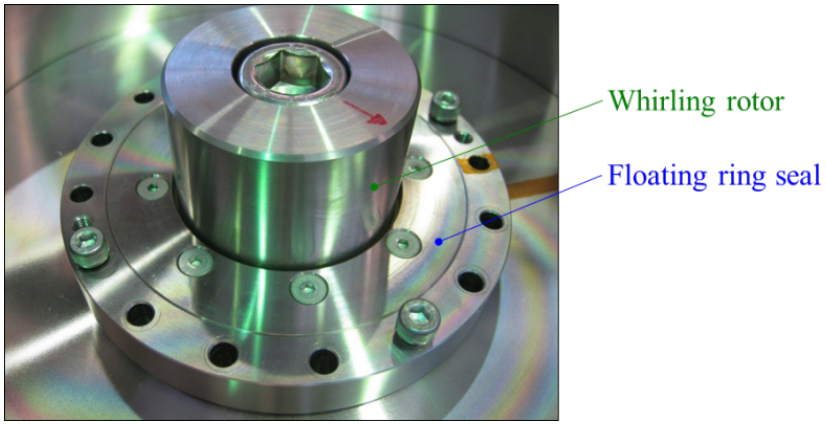

Fig. 9 FRS-inlet side view of the preassembly whirling rotor and FRS

A controlled seal clearance to the rotor should be maintained under operating whirling motion. To elucidate the structural behavior of FR caused by the whirling rotor, the FR behavior and the whirling motion of the rotor were measured with four displacement detectors which were set in the upper and lower portions over the x-axis and y-axis of this device, as shown in Fig. 10 and Fig. 11.

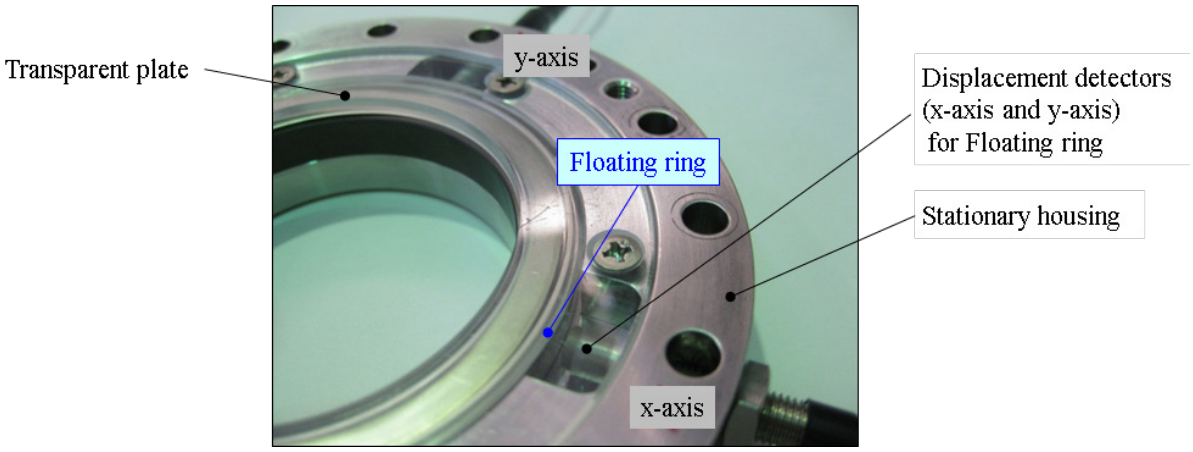

Fig. 10 Setup displacement detectors at the stationary housing for measuring FR behavior with whirling rotor

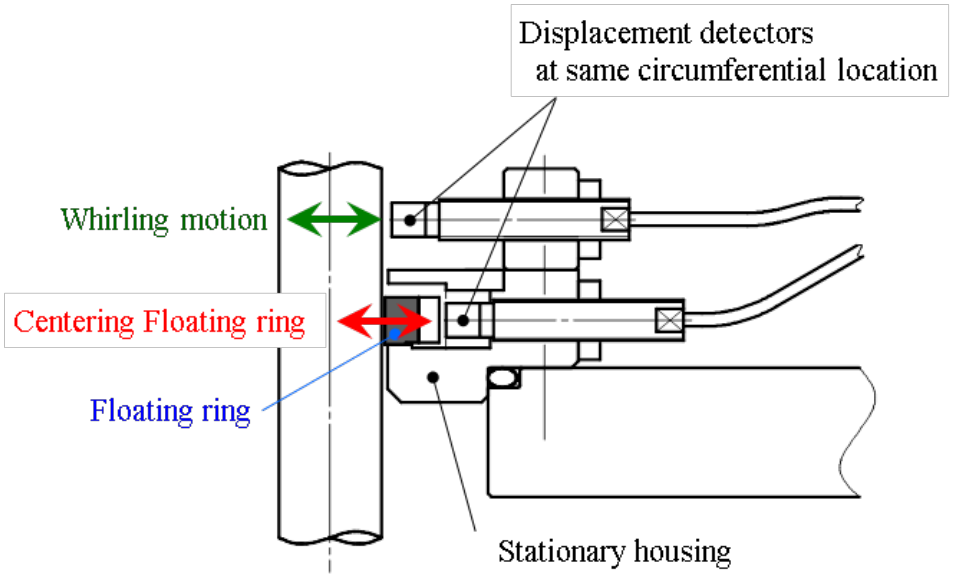

Fig. 11 Measuring the FR behavior and the whirling motion of the rotor at the same circumferential location

Experimental conditions

The FRS was the same size and had the similar configuration as that employed as a LOX seal in the LOX turbopump shaft seal system. The FR consists of an inner carbon ring for wear resistance and an outer Ni-alloy ring for strength and thermal contraction control. The FR is free to float in the radial direction to maintain a controlled seal clearance to the rotor under all operating conditions, as shown in Fig. 12. In addition, the FR is restrained from the spinning rotor with antirotation tangs that engage slots of the stationary housing. The axial force induced by differential pressure presses the FR against the stationary housing, and the secondary sealing surface is able to act as a static seal.

For the conditions of rotordynamic performance tests, the diameter of the rotor was 55 mm, and spinning speeds were 900 rpm (15 Hz), 1500 (25), 2100 (35) and 2700 (45). The working fluid was water at room temperature of approximately 330 K. Preswirl velocity was 0 m/s. The whirling motion of the rotor was translatory excitation, whirl frequencies were changed from frequency ratio (whirl/spinning) Ω/ω = -1.2 to +1.2, positive $+\Omega/\omega$ and negative $-\Omega/\omega$ indicating forward whirling motion and backward whirling motion, respectively whirl eccentricities of the rotor were 0.040 mm, 0.080, 0.120 and 0.160. Differential pressures were 0.5 MPa, 0.75, 1.0 and 1.25. FR was expected to center FR at the center of the spinning rotor and to maintain the controlled seal clearance, as shown in Fig. 13.

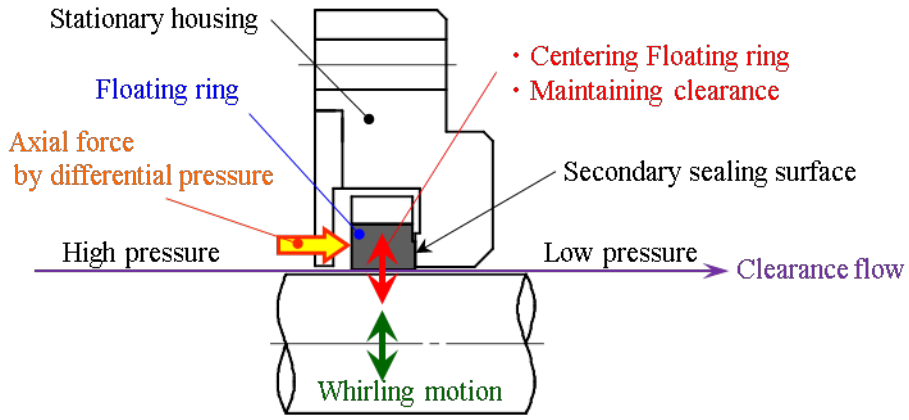

Fig. 12 FRS sealing mechanism, primary sealing surface (noncontact type), secondary sealing surface (contact type)

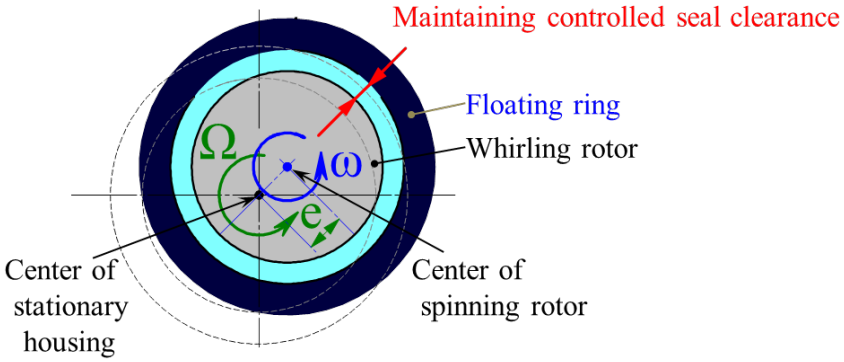

Fig. 13 Maintaining controlled seal clearance caused by centering FR at the center of the spinning rotor

EXPERIMENTAL RESULT OF FIXED RING SEAL

The experimental and analytic RD fluid forces were evaluated as qualitatively and quantitatively identifiable on all frequency ratios Ω/ω, as shown in Fig. 14.

The experimental tangential forces Ft were the curved lines from the origin of the coordinate axes, that is, the cross-coupled stiffness coefficients k were very small. The circumferential velocity in the seal strongly affected the tangential fluid force. However because the axial length / diameter = approximately 0.13 of fixed ring seal was smaller than that of annular seals [2], the cross-coupled stiffness coefficients k were very small.

The experimental radial forces Fr in the restoring effect increased in proportion to increasing whirl eccentricities caused by the Lomarkin effect. RD fluid forces were evaluated as being qualitatively and quantitatively similar.

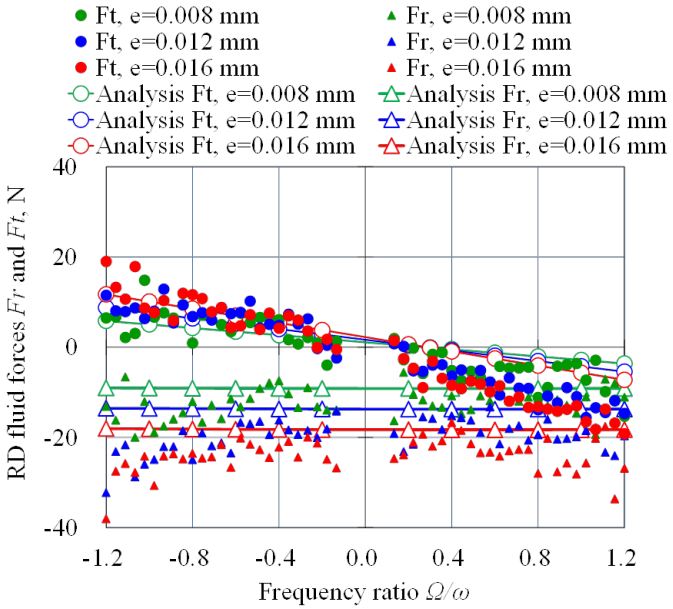

Fig. 14 Comparison between the experimental and calculated RD fluid forces for the fixed ring seal (dP=1.0 MPa, ω=2,700 rpm, Preswirl velocity=0 m/s)

EXPERIMENTAL RESULT OF FLOATING RING SEAL

Sealing characteristics

The sealing performance was insensitive to spinning speed, whirling motion and whirl eccentricity of the rotor, as shown in Fig. 15. Leakage of the FRS hardly vary relative to spinning speed of the rotor, that is, the increase of circumferential velocity due to the spinning speed have no impact on the axial velocity due to differential pressure under these conditions. Leakage linearly increased relative to the increase of square root of the differential pressure, as shown in Fig. 16. The sealing performance was sensitive only to the differential pressure but was insensitive to whirl frequency. From the above experimental investigations, the FR was able to be continuously repositioned with the whirling rotor, high whirl frequency and large whirl eccentricity, that is, to minimize leakage by maintenance of the radial sealing clearance. There were few wear tracks on the carbon sealing surface of FR. This indicates that it was easy for FR to reposition in the radial sealing clearance because of the low friction force working on axial secondary sealing surface. The repositioning and sealing performances were found to correspond to the intended design of the FRS.

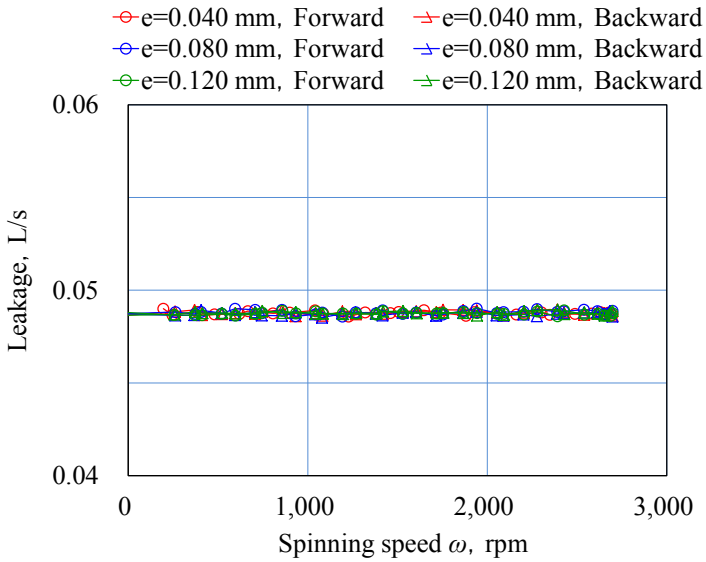

Fig. 15 Leakage with various spinning speed under many conditions of whirl eccentricities and directions of whirling motion (dP=0.5 MPa, Ω=15 Hz)

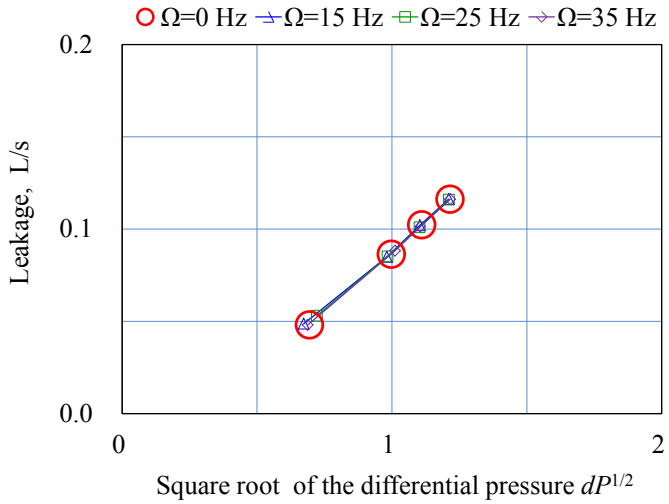

Fig. 16 Proportionally-increased leakage not relative to whirl frequency Ω (e=0.120 mm, forward whirling motion, dP=0.5 MPa, 1.0, 1.25, 1.50)

Effect of deferential pressure

The tangential and radial forces of differential pressure are shown in Fig. 17 (ω = 1500 rpm, *e* = 0.040 mm). The tangential forces *Ft* were the curved lines from the origin of the coordinate axes in the region of the damping effect, that is, the cross-coupled stiffness coefficients *k* were nearly zero, and the tangential forces *Ft* were not in the region of the destabilizing effect. The absolute value of the tangential forces *Ft* increased with the increase of differential pressure even if the frequency ratio *Ω/ω* was the same. The increase of differential pressure *dP* increased the axial load of the FR against the stationary housing, the high axial load increased the radial force required to reposition the FR, that is, the increase of the friction force induced by the high axial load caused the increase of the tangential forces *Ft*. The direct damping coefficients *C* (the slope of the tangential force curve) increased in proportion to the increase of the differential pressure within the low frequency ratio (approximately -0.4< *Ω/ω* <+0.4), but within the high frequency ratio (approximately *Ω/ω* < -0.4, +0.4< *Ω/ω*), the tangential forces *Ft* continued to be flat. Most of the radial forces *Fr* were in the region of the restoring effect, and not in the region of the inertia effect.

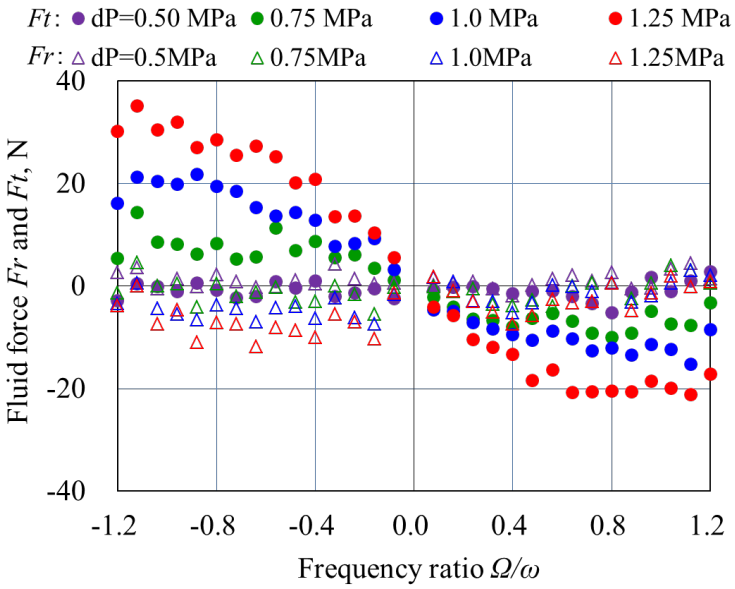

Fig. 17 Effect of the tangential fluid force (Ft) and the radial fluid force (Fr)with various differential pressure (ω=1,500 rpm, e=0.040 mm)

Effect of the whirl eccentricity

The radial and tangential forces increased with the increase of differential pressure *dP*, as shown in Fig. 18. The tangential forces *Ft* of whirl eccentricity *e* = 0.040 mm indicates the distinct curve, and *e* = 0.080, 0.120 and 0.160 indicated a similar tendency. The radial and tangential forces of the differential pressure 0.5 MPa were nearly zero, as shown in Fig. 18 (a). The axial load of the FR induced by the differential pressure 0.5 MPa was very low, that is, the radial force required to reposition the FR was negligible. The direct damping coefficients *C* increased with the increase of the differential pressure within the low frequency ratio (approximately -0.4< *Ω/ω* <+0.4), as shown in Fig. 19. Under the high differential pressure for the LOX turbopump, the large damping coefficient *C* should be expected to have a good impact on rotordynamic stability. The direct damping coefficients *C* were nearly zero under *dP* < 0.5 MPa because of the small axial load. The FRS should be employed under dP > 0.5 MPa because this small axial load has the possibility of fluttering (contact surface separation).

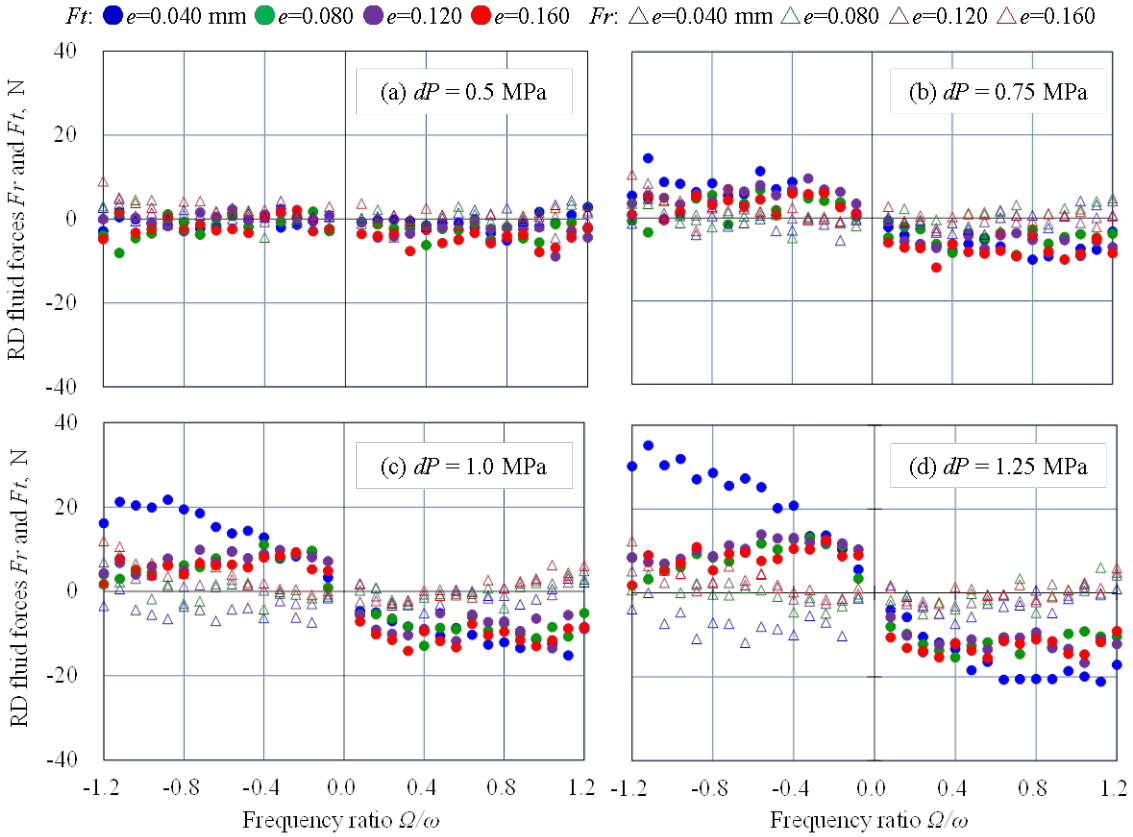

Fig. 18 Tangential force Ft due to the effect of differential pressure dP (ω=1,500 rpm)

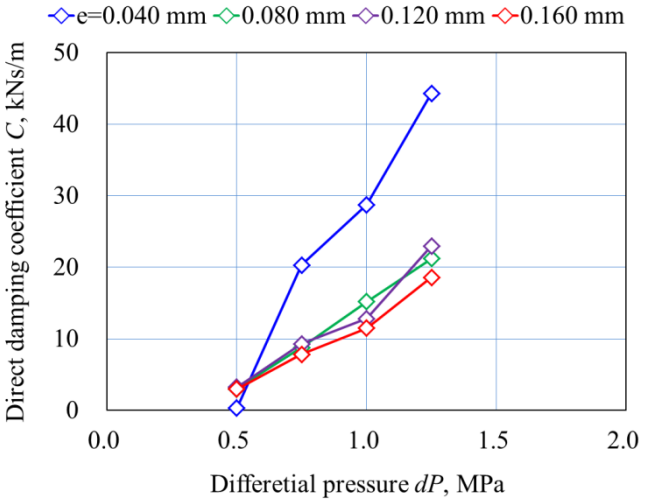

Fig. 19 Effect of the direct damping coefficient C versus differential pressure dP (ω=1,500 rpm, approximately -0.4 < Ω/ω < +0.4)

Effect of the seal clearance

The FR should maintain an initial controlled seal clearance to the rotor under all whirling rotor conditions to provide adequate leakage control. The displacement detector measured the FR behavior and the whirling motion of the rotor. The axial force induced by differential pressure presses FR against the stationary housing, that is, high axial loads increase the radial force caused by the friction force at the secondary sealing surface. The maximum dP = 1.25 MPa, the maximum Ω/ω = +1.2 (Ω = 30 Hz) and the maximum e = 0.160 mm were indicated that repositioning of FR with the rotor are the most difficult. The time-histories of the rotor and FR are shown in Fig. 20, the orbit of the rotor and FR is shown in Fig. 21. The FR was expected to have a time-lag between the whirling motion of the rotor and the response of FR because of the high friction force induced by dP = 1.25 MP; however, the FR was able to completely respond to the whirling rotor of the translatory excitation. In other words, the seal clearance did not vary with the above whirling rotor condition.

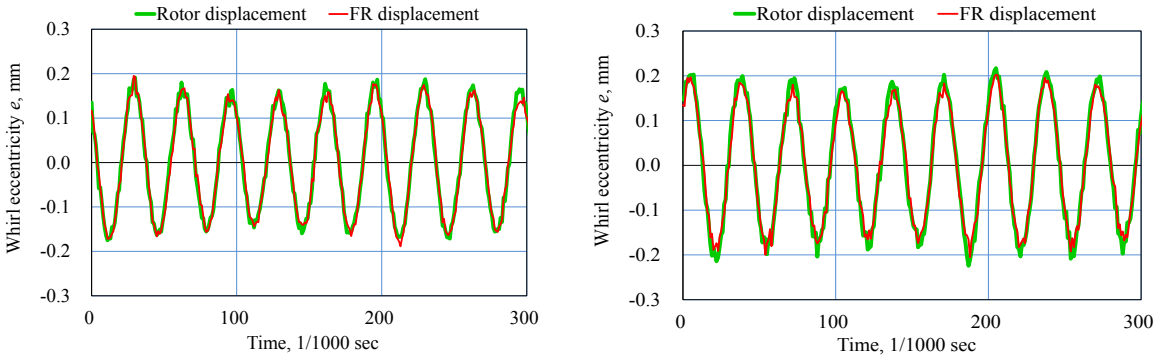

(a) Response to x-axis displacement (b) Response to y-axis displacement

Fig. 20 Response performance of FR to the whirling rotor under max dP, max Ω/ω, max e

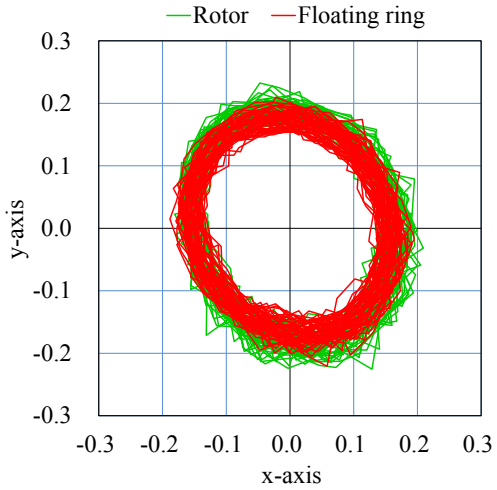

Fig. 21 Lissajous figures showing the orbit of the whirling rotor and repositioning of the FR under max dP, Ω/ω, e

DISCUSSION

Friction force for the secondary sealing surface

Through such rotordynamic performance tests, FR was found to be able to completely move with the whirling rotor, that is, the seal clearance did not vary under the whirling rotor conditions. The tangential force clearly increased in proportion to the increase of differential pressure, and no significant differences by the other parameters were shown. These results indicate that the forces measured by rotordynamic performance tests consisted essentially of the friction forces for the secondary sealing contact surface.

It must be difficult for the FR to move with the rotor because of the friction force loaded by the differential pressure. In the case of the forward whirling motion, the spinning rotor will attempt to translate in the positive direction of the tangential force Ft; however, the friction force acts on in the opposite-direction of the positive detection of Ft, that is, the friction force is measured as the damping force on the rotor. In addition, the tangential force Ft continued to be flat within the high frequency ratio Ω/ω. The high frequency ratio Ω/ω indicates that the sliding velocity of the secondary sealing contact surface is large.

Stribeck curve [9] was expressed the relationship between the friction coefficient μ, viscosity of the lubricant η, sliding velocity $2\pi e\Omega$, and the axial force by dP per unit length $(A \cdot dP)/L$, as shown in Fig. 22 and Eq. (10). This curve brilliantly captures the characteristics of various lubrication regimes, including boundary lubrication, mixed lubrication, and fluid film lubrication. Bearing characteristic number G (dimensionless number) increases with the increase of sliding velocity $2\pi e\Omega$, the zero point corresponds to static friction. In other words, friction coefficient μ varies with whirl frequency Ω. Boundary lubrication is characterized by little fluid in the secondary sealing contact surface under low whirl frequency Ω, and high friction coefficient μ. As the whirl frequency Ω increase, the secondary sealing contact surface will begin to separate and a fluid film begins to form.

The secondary sealing contact surfaces were manufactured by high-precision processing technology. The surface waviness is very small on the secondary sealing contact surface. Because of the effect of the surface waviness, etc., the inflow of the working fluid between the secondary sealing lines with whirl frequency Ω varied with the lubrication regime. Mixed lubrication has a very thin fluid film, and friction coefficient μ decreases sharply caused by the decrease of secondary sealing contact surface. The secondary sealing contact surface will continue to decrease with the increase of the whirl frequency Ω up to full fluid film and no contact surface. The friction coefficient μ will reach the minimum, and changes to fluid film lubrication. In the low whirl frequency Ω, the lubrication was in the boundary lubrication regime on the Stribeck curve. Under the high whirl frequency Ω, the lubrication changes from the boundary lubrication to the mixed lubrication, as shown in Fig. 23. The friction coefficient decreased with the increase of sliding velocity of the secondary sealing contact surface. The decreasing tangential forces Ft on the high whirl frequency Ω/ω, as shown in Fig. 18 (d) backward whirling motion, etc., may be explained by tribological behavior. Friction coefficient μ continued to be flat on the low bearing characteristic number G, and then begin to decrease. The decreasing tangential forces Ft indicated that the lubrication changes from the boundary lubrication to the mixed lubrication. In addition, the tangential force Ft continued to be flat at all whirl frequencies, as shown in Fig. 18 (a). This is caused by the small friction force of the small differential pressure 0.5 MPa. The lubrication regime will be the mixed lubrication.

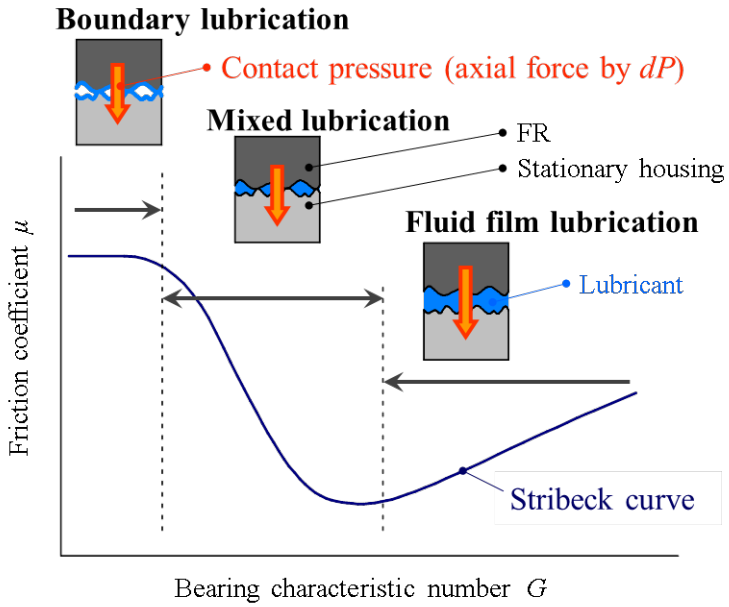

Fig. 22 Variation of friction coefficient μ with the sliding velocity 2πeΩ and differential pressure dP on Stribeck curve

$$G = \eta \frac{(2\pi e\Omega)}{(A \cdot dP)/L} = \left(\frac{2\pi\eta L}{A}\right) \cdot \frac{e}{dP} \cdot \Omega \tag{10}$$

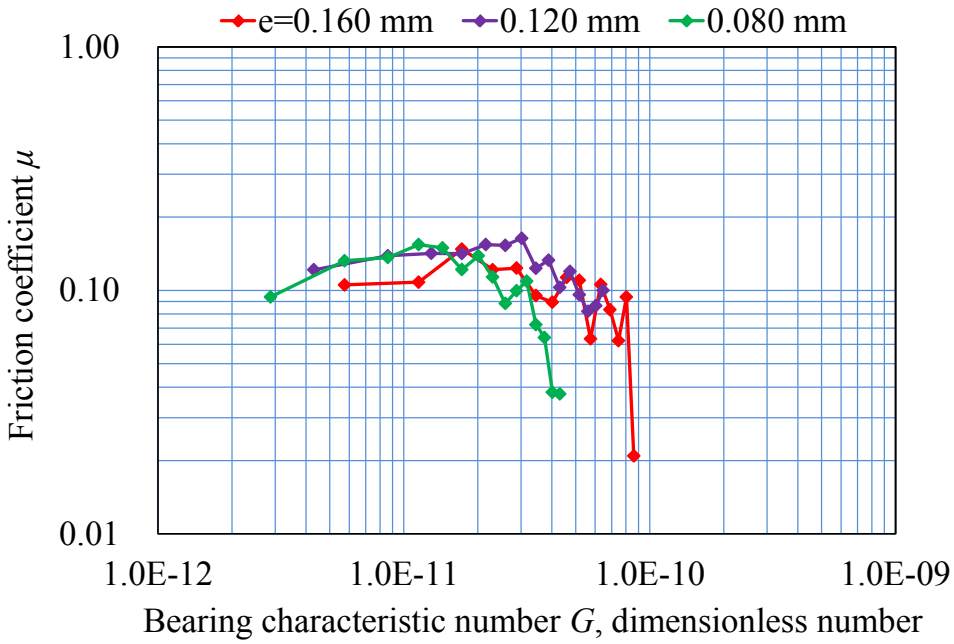

Fig. 23 Variation of friction coefficient μ with the translation to mixed lubrication (ω=1,500 rpm, dP=1.25 MPa, Fig 18(d) backward whirling motion)

CONCLUDING REMARKS

To obtain the RD fluid forces and the structural behavior of the FRS, rotordynamic performance tests were performed by using a rotordynamic test stand.

RD fluid forces of the FRS were lower than those of plain annular seals and were not significantly affected on the instability of the rotor. Because RD fluid forces were very small, most of the radial forces were in the region of the restoring effect, and most of the tangential forces were in the region of the damping effect. Circumferential fluid velocity in the seal (axial length of the seal) was found to have a significant effect on the stability of the rotor. The FRS has sufficient ability to center the FR at the center of the spinning rotor due to the fluid force required to reposition FR under the whirling rotor.

In the case of the forward whirling motion, the spinning rotor attempts to translate in the positive direction of the tangential force; however, the friction force acts on the direction of the opposite-positive detection of *Ft*, that is, the friction force acts on as the damping effect on the rotor. The damping coefficient *C* was in the positive region under the low frequency ratio, and increased in proportion to the increase of differential pressure. Under the high differential pressure for the LOX turbopump, the large damping coefficient *C* should be expected to have a good impact on rotordynamic stability.

The tangential force continues to be flat on the high frequency ratio Ω/ω. The increase of sliding velocity varies the lubrication regime. In the low frequency ratio Ω/ω, the lubrication was in the boundary lubrication regime on the Stribeck curve of the tribological behavior. Under the high frequency ratio Ω/ω, the lubrication changes from the boundary lubrication to the mixed lubrication. For FR behavior, the centering of the FR and the sealing performances of FRS were found to correspond to the intended design of the FRS. The FR was able to be continuously repositioned under all test conditions of high whirl frequency and large whirl eccentricity, that is, leakage was minimized due to maintenance of the radial controlled seal clearance.

Acknowledgments

Rotordynamic performance tests for FRS were performed by EBARA CORPORATION and supported by EAGLE INDUSTRY CO., LTD. The authors are indebted to these organizations for their cooperation.

NOMENCLATURE

ω	Spinning speed
Ω	Whirl frequency
Ω/ω	Frequency ratio
e	Whirl eccentricity
F	Fluid reaction force
Fr	Radial fluid reaction force
Ft	Tangential fluid reaction force
M	Direct added mass coefficient
C	Direct damping coefficient
K	Direct stiffness coefficient
m	Cross-coupled added mass coefficient
c	Cross-coupled damping coefficient
k	Cross-coupled stiffness coefficient

h	Fluid film thickness = Seal clearance
R	Rotor radius
u	Mean circumferential-velocity
w	Mean axial-velocity
t	Time
θ, z	Cylindrical coordinates
ρ	Density of flowing fluid
p	Pressure in seal
dP	Differential pressure
f_s	Seal friction factor
f_r	Rotor friction factor
V_s	Flow velocity relative to seal surface roughness
V_r	Flow velocity relative to rotor surface roughness
m_s, n_s	Empirical coefficient for seal
m_r, n_r	Empirical coefficient for rotor
G	Bearing characteristic number
μ	Friction coefficient
η	Viscosity of lubricant
A	Pressure receiving area of FR
L	Radial length of contact surface

REFERENCES

[1] NASA CR-135211, 1977, “Small, High-pressure Liquid Oxygen Turbopump”

[2] Iwatsubo, T., Sheng, B. C., and Matsumoto, T., 1988, “An Experimental Study on the Static and Dynamic Characteristics of Pump Annular Seals,” NASA CP 3026, pp. 229-251.

[3] Uchiumi, M., Kawasaki, S., Shimagaki, M., Yoshida, Y., and Adachi, K., 2012, “Integrated Design Method of Turbopump Sub-system for Suppressing Rotor Lateral Vibration,” Asian Joint Conference on Propulsion and Power, Xi'an, China, AJCPP2012-044.

[4] Oike, M., Nagao, R., Nosaka, M., Kamijo, K. and Jinnouchi, T., 1995, “Characteristics of a Shaft Seal System for the LE-7 Liquid Oxygen Turbopump,” AIAA-95-3102.

[5] Childs, D., W. and Kim, C.-H., 1985, “Analysis and Testing for Rotordynamic Coefficients of Turbulent Annular Seals With Different, Directionally-Homogeneous Surface-Roughness Treatment for Rotor and Stator Elements,” Trans. ASME. J. Tribology Tech., pp. 296-306.

[6] Iwatsubo, T. and Ishimaru, H., 1999, “A Study on Static and Dynamic Characteristics of Parallel-Grooved Seal,” Trans. Jpn. Soc. Mech. Eng., (in Japanese), 65(629), C, pp. 68-75.

[7] Hirs, G., G., 1974, “A Systematic Study of Turbulent Film Flow,” Trans. ASME. J. Lubr. Tech., pp. 118-126.

[8] Eguchi, M., and Maruta, Y., 2003, “Development of Rotordynamics Measurement System with Active Magnetic Bearings,” Proceedings of 10th Asia-Pacific Vibration Conference, Gold Coast, Australia, 1, pp. 115-120.

[9] Stribeck, R., 1902, “Die wesentlichen Eigenschanften der Gleit- und Rollenlager,” Zeitschrift des Vereins Deutscher Ingenieure, 46, pp. 1341-1348, 1432-1438, 1463-1470.